Causes and Triggers of Mass-Movements: Overloading

Short title: Causes and Triggers of Mass-Movements: Overloading

Causes and Triggers of Mass-Movements: Overloading

Alain Demoulin[a, b]

Hans-Balder Havenith[c]

[a]FRS-FNRS, Brussels, Belgium

[b]Unit of Physical Geography and Quaternary, ~~Département de Géographie~~Department of Geography, University of Liege, Liege, Belgium

[c]Department of Geology, University of Liege, Liege, Belgium

1 Introduction

Any review of the literature on landslides rapidly comes to the obvious conclusion that heavy rainfall and earthquakes, occasionally also volcanic eruptions, are the most cited triggers of landsliding in natural conditions. By contrast, slope overloading is more frequently considered a major direct cause of human-induced mass movements, as evidenced by the dominant use of the term to refer to anthropogenic loading in the engineering literature. However, there may actually be natural seismic and non-seismic landslides whose main trigger is overloading, whereas overloading is but one of several concurrent factors in many anthropogenic landslides.

Strictly speaking, slope overloading is defined as the addition of a load that increases the existing stress applied to a slope, more specifically to a weaker shear surface within the slope material, so that the latter's ultimate shear strength is exceeded and failure occurs. But we shall also consider many more cases hereafter, where a moderate surcharge load, though not able to initiate slope failure by itself, is nevertheless a potent cofactor of triggering. The added load is either static (e.g., accumulation of fill or waste on top of a slope) or dynamic, inducing transient instantaneous excess shear stresses (seismic loading, wave loading). High-amplitude dynamic stress build-up by seismic shaking, possibly also by storm wave impacts on coastal cliffs, typically results in failure-triggering overload, whereas more continuous low-amplitude dynamic stresses from traffic vibrations in, e.g., highway and railway embankments lead to long-term plastic strain accumulation and material fatigue and should then be considered a preparatory factor as well as, occasionally, the eventual trigger of slope instability.

Statistical information on the role of overloading in triggering mass movements remains so far limited. A report documenting anthropogenic factors of landsliding in Europe (Nadim et al., 2011) illustrates the difficulty of isolating overloading among triggers of mass movement. According to this report, about 10% of the events included in a database of 4000 historical fatal landslides in Norway were clay slides, from which one of three was unequivocally human-induced, with overloading, associated with landfill or cut-and-fill for road or railway construction, being one of the most frequent triggers. No mention however in this report of the predominant role of added snow weight in triggering natural snow avalanches (see, e.g., Ancey, 2001; Hao et al., 2018), which is nevertheless the most widespread mass movement hazard together with rockslide in the country's mountainous areas. The same report further states that, from a data set of 2112 historical landslides, rockfalls and mudflows in France, 934 events, mainly landslides, were exclusively or partly triggered by human-induced "change in geometry of the slopes and overloading of surfaces," their frequency significantly increasing from the 1970s onwards. As a third case study, Nadim et al. (2011) cite the Canton of Bern (Switzerland), where statistics about human-induced landslides since 1972 (strongly underrepresented in the database because most of them are of relatively small size and, consequently, not reported) indicate that 5% would have resulted from overloading, and 15% from construction works. Another study in urban areas of the Tizi-Ouzou province of Algeria came to the conclusion that, among 84 landslides recorded from 2000 to 2016, 26 (31%) were primarily caused by human factors related to overloading and large earthworks (Kab et al., 2018). By contrast, Laws and Murray (2011) highlighted a decisive preparatory effect of slope overloading by constructions on rainfall-induced landslides in two recently urbanized areas of New Zealand for only 3% (Eastern Bay of Plenty coastal area) and 0% (Wellington hillside suburbs) of the slides.

Although such numbers might suggest that overloading is overall a fairly minor trigger of mass movement, this judgment should be tempered by the following considerations: (1) some highly destructive overloading-triggered landslides have induced large numbers of casualties, such as the Verdal quick-clay landslide (Norway, May 19, 1893, 116 fatalities) and the Shenzhen landfill-related landslide (China, December 20, 2015, 77 fatalities); (2) as pointed out in the above Norwegian and French case studies (Nadim et al., 2011) and further confirmed by a global analysis of fatal landslides over the 2004–16 period (Froude and Petley, 2018), the relative frequency of human-induced landslides in general, and of those related to construction works in particular, significantly and steadily increased with time over the last few decades; (3) according to

the acceptation of the word *overloading* given above, which includes dynamic loading, a large part of natural mass movement events worldwide are directly involving this process as the main trigger, namely most (often highly damaging and deadly) earthquake-triggered landslides; and (4) beyond those cases where it is the principal trigger of mass movement, overloading often acts in a more modest or hidden way, e.g., coincident with other factors of landsliding (e.g., vegetation-related pore pressure changes), or as an aggravating factor in rainfall-triggered slope failures (Ashland, 2003; Demoulin and Glade, 2004; Laws and Murray, 2011).

2 Overloading and the balance between resistant and driving forces

In the traditional limit-equilibrium approach of slope stability, the role of overloading in triggering landslides is examined through the prism of the balance between the forces that tend to make a slope slip and those that allow it to resist movement, expressed by the safety factor F. A safety factor is calculated for any surface of weakness on which rupture has occurred, or might occur, within the sloping material. Based on the Terzaghi (1936) theory, the factor of safety is defined and calculated as

$$F = \text{soil shear strength}/\text{shear stress} = \left[C + \left(W_n - U\right) * \text{tg}\ \varphi\right] / W_t \quad \textbf{(1)}$$

where material cohesion (C), the component of material weight normal to the rupture surface (W_n) and pore pressure (U) contribute to the soil shear strength together with the angle of internal friction φ, while the component of material weight parallel to the rupture surface (W_t) is the driving stress (Fig. 1).

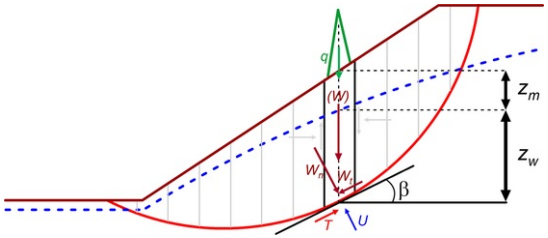

Fig. 1 Forces acting on a slice of the sliding mass in the method of slices for stability analysis. Rupture surface in red, water table in dashed blue, added load in green, interslice normal and shear forces as light gray arrows. (W): soil load; T: reaction of the slice base to the exerted forces; other labels: see Eq. (2) and related paragraph of the main text.

alt-text: Fig. 1

In the widely used infinite-slope model relevant to the analysis of shallow slides with a failure plane parallel to the sloping ground surface, the development of this equation yields (e.g., Gray and Megahan, 1981; Hammond et al., 1992; Selby, 1993):

$$F = \frac{c' + c_r + \left[q + \gamma_m z_m + \left(\gamma_{sat} - \gamma_w\right) z_w\right] \cos^2\beta \tan\varphi'}{\left[q + \gamma_m z_m + \gamma_{sat} z_w\right] \cos\beta \sin\beta} \quad \textbf{(2)}$$

where F is the non-dimensional factor of safety; c', the effective cohesion of the moist soil (kPa); c_r, the additional cohesion provided by the root mat of a tree cover (kPa); q, a surcharge load of any origin (kPa); z_m, the thickness of moist soil over the piezometric surface (m); z_w, the thickness of saturated soil over the analyzed shear surface (m); γ_m, the unit weight of moist soil above the piezometric surface ($\mathrm{N\,m^{-3}}$), equal to $\rho_m g$, moist soil density times acceleration of gravity; γ_{sat}, the unit weight of saturated soil ($\mathrm{N\,m^{-3}}$); γ_w, the unit weight of water ($\mathrm{N\,m^{-3}}$); β, the slope angle (°); and φ', the angle of internal friction of the moist soil (°). In this simple case of a rupture plane parallel to an infinite slope, one readily shows that the addition of a uniformly distributed surcharge load onto a slope will reduce the safety factor when the following criterion is satisfied:

$$c' + c_r > \gamma_w z_w \cos^2\beta \tan\varphi' \quad \textbf{(3)}$$

that is to say, when total soil cohesion is greater than the negative effect of pore pressure on soil strength, provided there is no change in cohesion or pore pressure associated with the overload (Ward, 1976). One notes that higher slope angles increase the probability of any surcharge diminishing F, as expected from the associated higher q_t/q_n ratio between the stress-increasing and strength-reinforcing components of the surcharge load q but, surprisingly, a lower piezometric surface or a high cohesion have the same effect. In the common instance of a loamy soil with $(c' + c_r) = 15$ kPa and $\varphi' = 20$ degrees and a piezometric surface 2–3 m above the shear plane, one calculates that every added load reduces the safety factor whatever the slope angle. By contrast, actual low cohesion of many potential rupture surfaces, such as bedding planes

dipping in the same direction as the slope surface, the weathering front interface, discontinuities within weathered rocks, regoliths, and non-clayey loose materials (Durgin, 1977; Speight and Isbell, 2009; Calcaterra and Parise, 2010) suggests that a surcharge load uniformly distributed over the slope will frequently increase stability of slope-parallel weakness planes. Moreover, while relative changes of F show a non-linear direct dependence on the added load, parametric variation studies have shown that the sensitivity of F to variations in q is overall fairly low (Gray and Megahan, 1981) (Fig. 2) and tends to decrease with increasing depth of the rupture plane (Mulder, 1991).

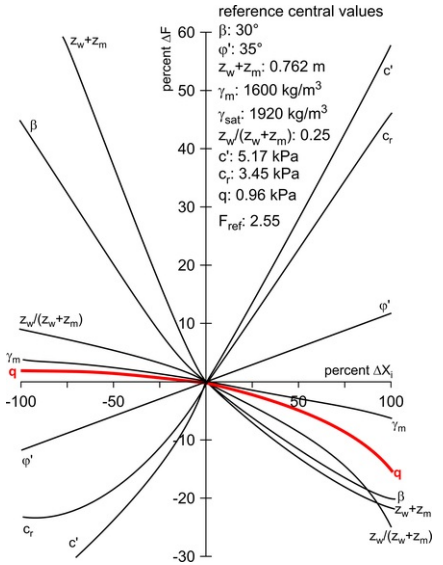

Fig. 2 Sensitivity of the factor of safety to changes in the variables of Eq. (2) (in black) and especially in added load q (in bold red) for a rupture surface at 0.762 m depth. Base safety factor was computed using the values listed in the figure. For each tested variable, the X axis expresses the departure from the central value as a percentage.

Redrawn after Gray D and Megahan W (1981) Forest Vegetation Removal and Slope Stability in the Idaho Batholith. USDA, Research Paper INT-271: Ogden, Utah, p. 23.

alt-text: Fig. 2

In the special case where the surcharge results from the growth of tall trees and, thus, also implies an increase in root cohesion Δc_r (see below), the condition for decreased F becomes

$$q > \Delta c_r \frac{(\gamma_m z_m + \gamma_{sat} z_w)}{(c' + c_{r0} - \gamma_w z_w \cos^2\beta \tan\varphi')} \quad \textbf{(4)}$$

Here, the condition explicitly defines a minimum value that the surcharge has to exceed in order to degrade F but, again, does not directly inform about the sensitivity of F to q.

Recent refinements to slope stability analysis in the frame of the infinite slope model correspond for instance to its expansion in 2.5D by including cohesion across the lateral surface of the slipping mass, in addition to that on the basal failure surface, in the expression of soil shear strength, considering also that lateral and vertical root cohesion differ in a way depending on tree species (Chiaradia et al., 2016).

However, another treatment of the stability analysis is required in the much more frequent case of deep and, especially, rotational landslides, where the dip of the failure surface varies along the slope. With regard to overloading, a more complex treatment is also needed to evaluate the effect of a localized extra load, depending on the particular location where it is applied in the slope or on top of it. The analysis of circular failure surfaces, supposed to represent the shape of the actual base surface of rotational slides, has been made possible from the time. Fellenius (1927) introduced the method of slices. In this method, the potential sliding mass is cut into slices of equal width and, based on the limit equilibrium equation, the safety factor is determined by considering only the forces acting on the slice bases, thus satisfying only the overall moment equilibrium (note that here the β angle of Eq. (2) represents the slice-dependent gradient of any considered rupture surface) (Fig. 1). In the following half-century, a number of method developments were proposed, which additionally involved interslice normal (Bishop's, Janbu's simplified methods) or normal and shear forces (e.g., Janbu's generalized, Spencer, Morgenstern-Price methods), then satisfying all equations of statics and both the force and moment equilibria (Krahn, 2003) (Fig. 1). Thanks to the ever increasing power of computers, currently available slope stability calculation software (e.g., FLAC by ITASCA™,

PLAXIS by Bentley Systems, SLOPE/W by SEEQUENT/Geoslope International, STABL by ENSOFT Inc.) allows users to analyze complex failure surface profiles in two dimensions and to incorporate a probabilistic analysis yielding estimates of the probability of failure and of the reliability of the calculated F (El-Ramly et al., 2002). More recently, a growing number of three-dimensional slope and landslide stability studies have also been completed (e.g., Huang and Tsai, 2000; Chen et al., 2003; Wan et al., 2016, 2018). In parallel, engineers developed the concurrent strength reduction approach to stability analysis, which has been implemented in both the finite element method (FEM) and the finite difference method (FDM) (Zienkiewicz et al., 1975; Naylor, 1981; Matsui and San, 1992; Griffiths and Lane, 1999; Yang et al., 2012, and many others). Based on the elasto-plastic computation of strain within a frictional slope, it works by incremental reduction of the original cohesion and friction angle parameters until slope collapse occurs, and presents the main advantages of automatically finding the critical failure surface (through the mapping of shear strain rates at collapse) and needing no assumption on interslice shear forces (Cheng et al., 2007). The strength reduction factor (SRF) yielded by this method is an exact equivalent of the safety factor of the limit equilibrium method (Griffiths and Lane, 1999).

The importance of the position of a surcharge load, be it a fill or a construction, for slope stability is clearly highlighted by Hutchinson (1977). Using the method of slices, he mapped influence lines describing the positive or negative impact of an additional load at any place along or above a slope. For a given weight and shape of the load and a fixed rupture surface, one simply maps the ratio:

$$F = \left(F_0 + \Delta F\right)/F_0$$ **(the *F* variable in the left member of equation (5) is different from the factor of safety *F*. This is why it MUST appear in a different font, as in our manuscript. We want it appear as an italic capital f in Lucida Calligraphy font.)** **(5)**

where F_0 is the pre-surcharge factor of safety for the considered rupture surface and ΔF the change in F *(this one is OK so.)* imposed by the added load, thus defining across the slope (or across an existing landslide) a neutral point (in 2D) or line (in 3D) with F *(here, please F in italic capital Lucida Calligraphy font.)* $= 1$, which separates the upslope part of the hillside where loading decreases the safety factor from the downslope part where it increases it. In passing, notice that, in Fig. 3A, Hutchinson (1984) shows the dependence of F *(again, please change font to italic capital Lucida Calligraphy.)* on α, the variable dip angle of the non-planar rupture surface, which however covaries with distance from the head of the surface and is thus a good proxy of the latter. Performing the analysis in drained and undrained conditions allows moreover defining an intermediate zone between the upper-located drained neutral line and the lower-lying undrained neutral line. This intermediate area experiences a short-term decrease in F *(this one is OK so.)* as long as undrained conditions prevail after extra loading, progressively giving way to reinforced stability of the slope once drained conditions are re-established (Fig. 3B). Slope surcharge issues have now also been dealt with in full 3D (e.g., Cheng et al., 2015) and using FEM (e.g., Sazzad and Haque, 2014).

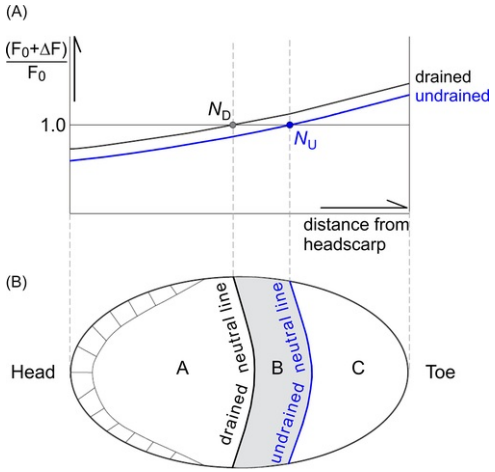

Fig. 3 Dependence on load position of the effect of an added load on the factor of safety. (A) Ratio of the factor of safety after vs before extra loading in function of alongslope position of the load for drained and undrained conditions. N_D and N_U are the neutral points (no change in F) in drained and undrained conditions, respectively. (B) Plan view of a landslide highlighting the intermediate zone (B) of time-dependent evolution of the post-loading factor of safety.

Redrawn after Van den Eeckhaut M, Poesen J and Hervás J (2013) Mass-movement causes: Overloading. In: Shroder J (Editor in Chief), Marston R and Stoffel M (Eds), Treatise on Geomorphology, vol. 7, Mountain and Hillslope Geomorphology, 1st edn, pp. 200–206, Academic Press: San Diego, CA, modified from an original figure of Hutchinson J (1984) An influence line approach to the stabilization of slopes by cuts and fills. Canadian Geotechnical Journal 21: 363–370.

alt-text: Fig. 3

All above methods refer exclusively to the static equilibrium of slopes. When a dynamic component of loading has to be taken into account, especially in the case of seismic (over)loading, two main approaches of slope stability may be envisaged. A first one is the Newmark Displacement analysis commonly used in seismic landslide analysis by geomorphologists, which will be discussed in the section devoted to seismic loading. However, civil engineers dealing with earth dam stability often use the alternative pseudostatic analysis (Seed, 1979) briefly outlined hereafter. The pseudostatic analysis is a static limit-equilibrium method incorporating a horizontal earthquake-induced inertial force applied to the potential landslide body, and delivering a classic F estimate (Bray and Travasarou, 2011). The pseudostatic inertial force is expressed as the product of the weight of the slipping mass and a seismic coefficient k whose value, generally taken between 0.1 and 0.2, depends on magnitude and distance of the design earthquake. Based on a conservative estimate of the acceptable seismic displacement of the slope, Hynes-Griffin and Franklin (1984) suggested to take k = half the peak ground acceleration on bedrock at the site. More recently, using 688 ground motion records, Bray and Travasarou (2007, 2009) established an empirical relation between the potential seismic displacement of the slope, the seismic coefficient k_y at failure, the fundamental period of the sliding mass, ground acceleration at the site and earthquake magnitude, which they can solve for the value of the yield coefficient associated with the size and exceedance probability of the seismic displacement acceptable for a particular engineered slope, and adapted to the design earthquake. In such studies, engineers also carefully estimate whether ground shaking may entail a significant loss of strength of slope material (e.g., due to the presence of liquefiable layers), thus imposing the use of dynamic strength parameters lower than their static counterpart.

3 Types of overloading

We present hereafter a review of the most important settings and mechanisms that can involve overloading-triggered landsliding or where overloading at least significantly contributes to the occurrence of landslides.

3.1 Overloading by higher-located slides

Though not very common, a number of cases have been recorded where natural overloading acted as the trigger of major landslides on steep mountain slopes. In these cases, an instantaneous high to very high load was applied by failure of the upslope part of the mountain causing rock or debris slide or flow ~~and~~that overloaded either the crown and upper part of a lower-located dormant landslide or the close-to-failure lower part of the mountain side. Thus, while any usual landslide trigger of mountainous regions (e.g., high rainfall, snowmelt, gravity, postglacial stress relaxation) initiates a first, sometimes minor, mass movement, the latter's load is the direct cause of the slightly delayed (by minutes to months) secondary larger reactivation or new landslide event.

The reactivation in 1974–75 of the Manti landslide on the western flank of the Wasatch Plateau, Utah, is a typical example of such a process (Fleming et al., 1988). In June 1974, probably in connection with the rapid melting of a snowpack, minor rock slumps and debris flows ran down the southern rim of the Manti Canyon. While much of the material was deposited at the base of the ~ 30 m high steep slope, part of it mixed with meltwater and flowed about 1 km farther downslope, where it stopped on the head of the large dormant Manti landslide (Fig. 4). Directly loaded by an estimated ~ 6500 m^3 of debris and probably also affected by a 10-fold load of material upslope from its crown, the upper part of the old landslide, itself saturated by meltwater, started soon to respond to the surcharge and excess pore water pressures, with cracks opening and propagating downslope at a rate of 4–5 m/h so that the landslide mass, inactive for decades beyond localized creep motion, began to move. In the first weeks, only the previously creeping upper sector of the landslide moved more actively but, in the next melting season (June to August 1975), cracks and displacements propagated downward and affected the entire landslide down to its toe along the Manti Creek, before it finally stabilized in the late spring of 1976. Displacement rates peaked at ~ 1 m/day in the upper part of the landslide, locally with a total displacement of more than 40 m, and at 3.1 m/day in the landslide toe area.

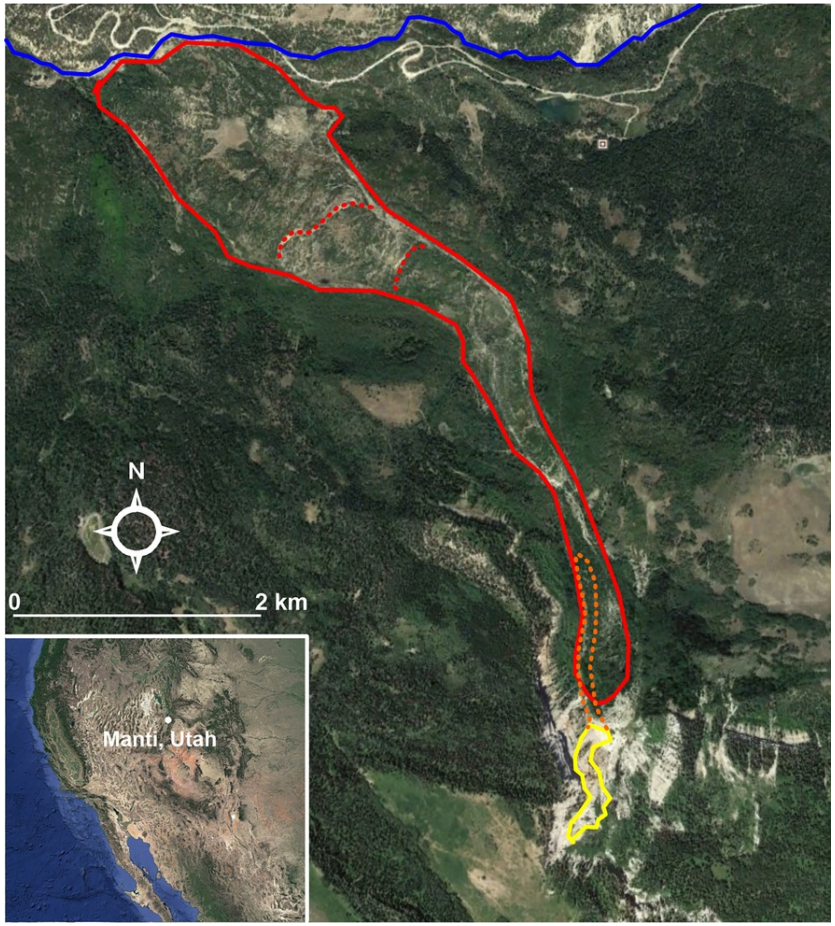

Fig. 4 Reactivation in 1974 of the dormant Manti landslide, Wasatch Plateau, Utah, after its head was loaded by minor rock slumps originating in the upstream part of the Manti canyon. Initial June 1974 rock slump is outlined in yellow, associated debris flo in dashed orange, dormant and reactivated Manti landslide in red.

Image 18.08.2015: © Google Earth.

alt-text: Fig. 4

The role of overloading in such multistage landslide events is sometimes less consensual. Starting with a rockslide that mobilized 3–4.5 million m^3 of material detached from the mountain top along a preexisting fracture, the Xinmo (Sichuan, China) landslide of June 24, 2017, rapidly developed into a huge rock and debris avalanche mobilizing a further 4.3–5 million m^3 of old landslide deposits lower in the slope (Su et al., 2017; Fan et al., 2017). The delay between the moment when the initially failed rock mass first hit the ground and the time when the main debris slide started to move has been estimated at 46 s from their record at a nearby seismic station (Su et al., 2017). In total, 8–13 million m^3 of debris are estimated to have reached the valley bottom, blocking the river over 2 km and causing ~ 80 fatalities. All authors agree on the factors and trigger of the initial rockslide, which was (i) prepared by the long-standing weakening of the ridge crest caused by the very close 1933 Diexi earthquake and later strong earthquakes, (ii) facilitated by the structural dip parallel to the slope, and (iii) finally initiated by a low-intensity but long-duration rainfall episode (Su et al., 2017; Fan et al., 2017; Wang et al., 2018). By contrast, their respective interpretations of the mechanisms at play in the second stage of the event differ slightly. Whereas Fan et al. (2017) only mention scraping, entraining, and pushing of the old landslide deposits by the highly energetic hurtling rock mass, Wang et al. (2018) suggest that the impact of the falling rocks rapidly turned a part of the sliding body, essentially loamy soils with few gravels and boulders, into clastic flow, and Su et al. (2017) explicitly invoke, beyond scraping and shoveling, overloading of the mid-slope loose sediments by the failed rock mass. Although the latter interpretation is quite plausible (through the intervention of loading-induced excessive pore pressures in the sediments), this example underlines how difficult it may sometimes be to distinguish between multiple possible triggers of landsliding.

3.2 Overloading by high soil water content

The increase in soil water weight with heavy rainfall or rapid snowmelt, but also with leaking water pipes, canals, irrigation systems, reservoirs, and septic tanks, and rising groundwater table is sometimes mentioned as (e.g., Selby, 1993), or proved to be (Kazmi et al., 2017), a cause of slope (over)loading. However, one commonly considers that the main effect of elevation of the water table is an increase in pore pressure that proportionately decreases the strength of the slope material, thus tending to trigger landslides (e.g., Wieczorek, 1996). Yet, beyond other effects of changes of water level in the soil (change in suction, seepage pressure, lubrication of soil discontinuities), the impact of the weight of additional water combines, though in varying proportions, with the effect of pore pressure to decrease the factor of safety in all cases. This is best illustrated by rewriting Eq. (2) to decompose the factor of safety into its three components according to Iverson (1991):

$$F = F_f + F_w + F_c = \frac{\tan\varphi'}{\tan\beta} - \frac{\gamma_w z_w \cos^2\beta \tan\varphi'}{\left(\gamma_m z_m + \gamma_{sat} z_w\right)\cos\beta\sin\beta} + \frac{c' + c_r}{\left(\gamma_m z_m + \gamma_{sat} z_w\right)\cos\beta\sin\beta} \quad \textbf{(6)}$$

where F_f, F_w, and F_c include the respective contributions to soil shear strength of the gravity forces, the pore pressure, and the cohesion. This reformulation also clearly highlights the origin of the criterion of Eq. (3) for the effect of an added load on F, except that, when this extra load is ground-saturating water (included here in the term $\gamma_{sat}\, z_w$), it also involves a change in the pore pressure term $\gamma_w z_w$. Expressing the change in F caused by a rise in water table, rewriting

$$\gamma_{sat}\, z_w = \left(\gamma_m + \gamma_w\, p\right)\, z_w \quad \textbf{(7)}$$

with p equivalent to the saturated porosity of the ground, and rearranging the relation, one obtains the following criterion for a decrease in F

$$p\, \left(c' + c_r\right)\, \left(z_{w1} - z_{w2}\right) < \gamma_m\, Z\, \left(z_{w2} - z_{w1}\right)\, \cos^2\beta\, \tan\varphi' \quad \textbf{(8)}$$

where $Z = z_w + z_m$, and z_{w1} and z_{w2} are the initial and final levels of the water table, respectively. Eq. (8) evidences that the factor of safety is reduced in all cases where $z_{w2} > z_{w1}$, whatever the contributions of water load versus pore pressure in this decrease.

3.3 Overloading by dense tree cover

Vegetation, and especially a dense tree cover, is another factor for which (over)loading is commonly considered one of many effects on landsliding. Although their net result actually tends toward the stabilization of most slopes (Greenway, 1987), many of the interacting hydrological and mechanical processes governing the vegetation—soil interactions may be either beneficial or adverse to slope stability:

(1) interception by the foliage is beneficial in that enhanced evapotranspiration and water absorption reduce infiltration but excessive depletion of soil moisture may finally lead to soil cracking and higher infiltration capacity;

(2) likewise, roots extract water from the soil but in the same time the stem-root system increases soil permeability and infiltration capacity;

(3) mechanically, the tree root system is beneficial because it increases the soil shear strength and vertically anchors the soil mantle into firmer material at depth (with a balance between both effects depending on tree species). But, in the case of a shallow root system strengthening the soil mass down to a mechanical discontinuity, such as a sharp weathering front, but not across it, a large contrast in strength is created and the risk of failure as a whole of the mass above the discontinuity is increased;

(4) vertical anchoring by the root system generally stabilizes the slope but it also more efficiently transmits to the soil the dynamic load of storm winds blowing in the trees and, once its buttressing effect on the upslope soil mantle is overcome or a tree is uprooted by a storm, it results in the creation of entries for concentrated water infiltration into the soil and increased slide probability;

(5) finally, the surcharge caused by the weight of the tree cover is decomposed as the combination of the normal and downslope components, with their antagonistic effects on slope stability and their gradient-dependent balance.

In general terms, it must also be stressed that the impact of the tree weight component on slope stability is strongly dependent on the location of the surcharge on the slope. In particular, in the case of the concave-up nascent weakness surface that precedes rotational landsliding, its gradient β, and thus also the negative effect of a surcharge load on stability, are highest and most destabilizing upslope (see Eq. (6)), whereas low, then reverse gradients of the rupture surface close to the slope toe result in a tree surcharge there improving the safety factor (e.g., Genet et al., 2010).

To evaluate the potential slope overloading role of tree cover, a main issue is to obtain reliable estimates of the actual intensity of the surcharge it can impose on the soil and to check how it compares with other vegetation impacts. Dubious figures as high as 70 kPa have indeed been mentioned for the load of large Douglas-fir trees (Gray, 1978), and estimates in the order of 3–6 kPa are commonly encountered in the geomorphological literature on landslides (e.g., 3.8–5.2 kPa for Sitka spruces in Alaska (Wu et al., 1979); 3.5 kPa for pine trees in the Alps (Van Asch et al., 1989); 2.94 kPa for a densely planted pine forest in Korea (Kim et al., 2013)). By contrast, equivalent estimates are systematically lower in the forestry literature.

Much attention has been dedicated by forest engineers to the estimation of the forest biomass. In most publications, estimates refer to the dry above-ground biomass (AGB) in tons per hectare, with published values covering a variable part of the components of a forest stand (large and small tree stems, branches, leaves, shrubs, lianas). Most recent studies of tropical rainforests provide estimates of dry above-ground biomass in the order of 200–600 t/ha, which correspond to equivalent uniform surcharge loads of 0.2–0.6 kPa, with consistent results obtained from field measurements of felled trees, field-based allometric models (e.g., Yamakura et al., 1986; Cummings et al., 2002; Lewis et al., 2013; Ioki et al., 2014), and remotely sensed, e.g., LiDAR-based, regional estimates (e.g., Xu et al., 2017). As for temperate coniferous or broadleaf and boreal forests, their dry AGB generally corresponds to loads falling in the 0.2–0.5 kPa range (Szwagrzyk and Gazda, 2007; Sun et al., 2011; Chiaradia et al., 2016). However, in order to estimate the actual load of a forest on a slope, one needs to convert dry AGBs in fresh AGBs including the water content of the living vegetation. Measured fresh-to-dry ratios of above-ground biomass are commonly slightly lower than 2, in the order of, e.g., 1.7–1.9 for tropical rainforests (Higuchi et al., 1994) or 2.1 for Norway spruce in Sweden (Johansson, 1999), suggesting that true maximum equivalent uniform forest loads do not exceed ~ 1.2 kPa. Note also that adding the weight of the rooting system to the load does not significantly alter the estimates as the root-to-shoot ratio is < 0.2, for example 0.17 for *Pinus* spp. in S. Brazil (Sanquetta et al., 2011).

However, especially for multistoried intertropical rainforests, equivalent uniform vegetation loads should not conceal the fact that very large individual trees of the overstory may impose significantly higher local surcharge on the slope. For example, Gonzalez de Tanago et al. (2018) estimated a weight of ~ 37 t for a *Buchenavia macrophylla* in Peru, Yamakura et al. (1986) obtained a weight of ~ 43 t for a 70.7 m high *Shorea laevis*, and Fayolle et al. (2013) ~ 70 t for an *Entandrophragma cylindricum* in SE Cameroon. Distributing such masses on a realistic root plate area (i.e., the surface where thick, structural, rapidly tapering roots extend radially from the stem) of ~ 370 m^2 derived from the measured ~ 2-m stem diameter of these tall trees at breast height (Coder, 2014), and considering a fresh-to-dry AGB ratio of 1.8, one gets local surcharges of 1.8, 2.1, and 3.3 kPa, respectively.

Such surcharge values, and still more their fraction that really contributes an additional shear stress, are low in comparison with other effects of tree cover on slope stability. In particular, the reinforcement of the soil by the roots has been largely documented. Increase in shear strength in the order of 10–25 kPa through root reinforcement has been measured for poorly cohesive sandy soils (Ziemer, 1981; Maffra et al., 2019) as well as for mixed soils on steep slopes (Ekayanake et al., 1997). However, being strongly dependent on the root cross-sectional area per unit shear area, this increase in soil cohesion is spatially highly variable at the intra-stand scale and has been observed to diminish laterally with distance from the stem (Schwarz et al., 2012) and vertically with depth (e.g., Ji et al., 2012). Nonetheless, given a difference of more than one order of magnitude between the surcharge and root reinforcement effects, it is therefore not surprising that most studies considering the effect of tree loading on slope stability come to the conclusion that, though measurable, it is in general secondary to other vegetation effects, especially soil strengthening by the root system (Gray and Megahan, 1981; Abernethy and Rutherfurd, 2000) but also pore pressure alteration (Simon and Collison, 2002).

3.4 Overloading and quick-clay landslides

Quick clays are (silty) clays accumulated in marine environments, mostly in relation with isostatically depressed areas around the ice caps of Europe, Asia, and North America, where they acquired an open flocculated structure that owed its strength to mineral layer bonding through cations (Geertsema, 2013). After the melting of the ice caps, isostatic rebound brought the clays on land, where they were either exposed or buried beneath other sediments. There, whatever their position with respect to the ground surface, the bonding cations were progressively leached away by percolating freshwater. From that moment, the saturated porous clays preserved their strength but were in a metastable state that makes them highly prone to collapse. Even moderate loads are then likely to cause overloading and disturb the unstable structure of such clays, leading to their remolding, drastic decrease of strength (the degree of sensitivity of the clays is expressed by the ratio of their strength before and after remolding—Torrance, 2012), and static liquefaction (the collapse of the grain structure induces a phase separation, which in turn causes the layer at the base of the landslide to flow). This is the beginning of landsliding, which may occur on very gentle slopes and generally extends retrogressively, developing into very large landslides.

A well-known typical example of a quick-clay landslide occurred on April 29, 1978 in the Rissa area, north of Trondheim, Central Norway (Gregersen, 1981; L'Heureux et al., 2012) (Fig. 5). Covering an area of ~ 33 ha, it mobilized about 5–6 million m^3. The two-stage landslide started along the southwestern shore of Lake Botnen, where it was triggered by a 700 m^3 earth fill aimed at gaining farmland area. The surcharge caused by the fill initially caused a relatively minor failure in the weathered material of the bank of the lake. Indeed, the fill was barely placed down when a ~ 80 m long, ~ 20 m wide piece of the shoreline including part of the fill, slid into the lake. In this first stage of the event, the landslide developed through a series of minor slides, each of them associated with liquefaction of the clay, proceeding retrogressively at a moderate pace over a timespan of 40 min to cover a < 3 ha wide area. At that time, the landslide had the shape of a 450 m long, a few meter deep, narrow pit as almost all the sliding material had been liquefied and had run down into the lake. Then, in an unexpected second stage of the event, a large 3-ha-wide flakeslide adjoining the head of the previously excavated area commenced to slide monolithically, then to liquefy, flowing not toward the pit axis but laterally down to the lake at a moderate speed estimated in the order of 3–5 m/s by an eye witness. It immediately caused a sequence of retrogressive flakesliding, some chunks of land moving now at speeds up to 10 m/s, which took only 5 min to extend the landslide scar along the hillslope foot by more than 1 km before the motion came to rest. Moreover, further damage was caused in Leiraveien, at the other end of the lake, which was reached by a 3 m high seiche wave (Martin et al., 2017).

Fig. 5 The April 29, 1978, Rissa (Central Norway) quick-clay landslide. The red arrow locates the position of the earth fill that initially triggered the failure of a relatively small landslide (yellow ellipse), which then rapidly evolved retrogressively.

Photograph courtesy of Aftenposten.

alt-text: Fig. 5

3.5 Seismic loading

Seismic loading is a special case of overloading where not only the added load itself but also its dynamic character are decisive in triggering landslides of all possible types. A recent compilation of landslide mobilization rates from 116 study areas worldwide suggests that, at the global scale, 30–40% of the slope material mobilized in mass movements would result from earthquake-triggered landslides, a figure rising to ~ 70% in regions of high seismicity (Broeckx et al., 2020). Seismic overloading is therefore a major cause of landsliding, whose forecasting however remains as elusive as the prediction of earthquakes. As earthquake-triggered landslides are treated in detail elsewhere, we deal here only briefly with the specific issue of how dynamic loading by propagating seismic waves acts as a surcharge responsible for slope failure.

From statistics of landslides in seismic areas, Keefer (1984) concluded that, depending on the type of mass movement, a minimum earthquake magnitude of 4–5 is required in order that oscillating ground motions produced at the passage of seismic elastic waves can cause landsliding. In this regard, the determining factor is the acceleration imposed to the ground by the travelling waves. Cycle after cycle, whenever acceleration exceeds the threshold required to overcome ground friction, micro-displacements progressively concentrate on the weakest potential rupture surface in the ground until the cumulative downslope displacement of the block above this surface reaches a critical value above which it leads to failure. Used as a criterion to assess the probability of earthquake-triggered slope failure in a dynamic approach of slope stability, this critical pre-slide displacement D_N is the key parameter because it incorporates the effects of both the seismic stress applied to the ground and the strength of the latter. It is generally called the Newmark displacement because Newmark (1965) was the first to propose this kind of quasi-dynamic analysis, however not yet a fully dynamic one such as those now achieved through dynamic numerical modeling considering also, e.g., ground viscosity and dynamic changes in soil strength (through strain softening) (e.g., Wakai et al., 2010; Gerolymos, 2010; Huang et al., 2016). In order to determine D_N, the resistance to motion of the slope material is expressed through the estimation of the critical acceleration a_c needed for strong ground motion to initiate sliding as

$$a_c = (F - 1)\,\mathrm{g}\,\sin\,\alpha \tag{9}$$

where F is the safety factor of the weakest potential rupture surface, g the acceleration of gravity and α, the thrust angle, is the angle to the horizontal of the initial sliding direction of the moving mass center of gravity (i.e., simply the slope angle in an infinite slope model) (Jibson, 1993). The second information needed to estimate D_N is the acceleration-time history of the slope during the earthquake, from which the cumulative inertial displacement of the slide mass is obtained by integrating twice the spans where the curve runs above the critical acceleration level. Whereas peak ground acceleration is a rather poor proxy for the shaking content of an earthquake, Arias (1970) devised a practical measure of total seismic shaking intensity, called Arias intensity I_A. Widely used in D_N estimations, it is based on the integral of the time-domain ground acceleration and reads as

$$I_A = \frac{\pi}{2g}\int_0^d [a\,(t)]^2 dt \tag{10}$$

where a is the ground acceleration and d the duration of strong ground shaking, I_A being then expressed as a velocity. Obviously, direct calculation of D_N and I_A for a given slope requires an accelerogram obtained on, or close to, site but such data are not available in most cases, thus preventing direct determination of D_N. This urged Jibson (1993) to propose a simplified Newmark's method based on empirical relations.

To overcome the difficulty, Wilson and Keefer (1985) and Wilson (1993) firstly used strong motion data from several earthquakes in California to empirically confirm the theoretical form of, and parameterize, the equation that relates I_A to the earthquake magnitude and the distance from earthquake to site, proxy for the geometric spreading of the elastic wave energy. Wilson (1993) also added a third term for the anelastic attenuation of the seismic waves, so that the relation obtained for I_A—representative of the surcharge applied to the slope by its dynamic loading—is expressed as (simplified after Wilson, 1993)

$$\log I_A = M_w - 2\log R - kR - 3.99 + \varepsilon \quad \textbf{(11)}$$

where M_w is the earthquake moment magnitude, R the distance from the seismic source to the slope under study (including a term allowing for the fact that the source point of peak motion may lie anywhere on the fault rupture surface), k the coefficient of anelastic absorption, and ε the residual error term. This relation can be used to map the Arias intensity applied to slopes everywhere in the shaken area independently of the availability of local accelerograms (e.g., Garcia-Rodriguez et al., 2008). Moreover, amplification factors may also be applied to the calculated Arias intensity in order to account for lithologic and topographic site effects (Ashford et al., 1997; Garcia-Rodriguez et al., 2008; Torgoev et al., 2013).

Secondly, based on growing data sets of strong motion records, Jibson and Keefer (1993), Jibson et al. (1998), and Jibson (2007) fitted multivariate models that indirectly estimate D_N from its relation with I_A and a_c. Relying on 875 Newmark displacements selected from strong motion data of 30 worldwide earthquakes (20 in California, 10 in the rest of the world) to evenly cover the meaningful range of a_c, the empirical relation provided by Jibson (2007) reads as

$$\log D_N = 2.401\log I_A - 3.481\log a_c - 3.230 \pm 0.656 \quad \textbf{(12)}$$

with D_N in cm, I_A in m/s, a_c in g's, and a coefficient of determination $R^2 = 0.71$.

More recently, using a worldwide data set of strong motion records, Hsieh and Lee (2011) showed the slightly modified equation

$$\log D_N = C_1\log I_A + C_2 a_c + C_3 a_c \log I_A + C_4 + \varepsilon \quad \textbf{(13)}$$

with C_1 to C_4 = regression coefficients, performs better in their case (1343 records from 6 earthquakes, $R^2 = 0.89$).

However, stand-alone estimation of D_N is of limited help as long as no threshold Newmark displacement is defined for slope failure. Two approaches have been used to solve this issue. In some studies, a critical D_N has been empirically estimated, e.g., in the order of 5–10 cm for landslides in California (Wieczorek et al., 1985; Keefer and Wilson, 1989). As these estimates strongly depend on local conditions and the type of slide, their relevance beyond the region of definition may be questioned. Instead, Jibson et al. (1998) consider that modeled Newmark displacements provide an index to highlight relative probabilities of slope failure in the mapped area (e.g., Garcia-Rodriguez et al., 2008; Garcia-Mayordomo et al., 2009; Ma and Xu, 2019).

The simplified Newmark method is an effective approach of seismic (over)loading and its potential to cause slope failure. Nevertheless, one should keep in mind the many assumptions acknowledged by Newmark (1965) (e.g., rigid-block approximation, similar static and dynamic shear strength of the material, strain-independent constant critical acceleration) and other factors unaccounted for (e.g., the amplitude and phase relationships between the in-plane slope-parallel and slope-normal components of the seismic acceleration of the ground—Ingles et al., 2006; Brain et al., 2015).

3.6 Dynamic loading of cliffs by storm waves

Whereas many authors have suggested that infinitely repeated low-magnitude cyclic loading of the wave impacts may cause fatigue phenomena and progressively reduce the strength of cliff rocks through microcrack growth, thus contributing to cliff collapse (e.g., Adams et al., 2005), field measurements of the microseismic ground displacements caused by these impacts showed that they are not enough energetic to trigger cliff failure and mass movements (Brain et al., 2014). However, laboratory experiments have shown that the pressure of wave impact propagates into the cracks of the rock where they build up very large loads in case of water-filled cracks, and even higher pressures in partially filled cracks, where pressure travels fast and is barely attenuated in the air of the crack deep into the rock mass, leading to the removal of blocks and weakening of the cliff face (Wolters and Müller, 2004). Moreover, ordinary wave impacts are capable of eroding the cliff's foot in weak rocks (e.g., chalk, poorly to moderately cemented sands), resulting in the development of notches that prepare future landsliding (e.g., Collins and Sitar, 2008).

By contrast, dynamic loading by (subharmonic) infragravity waves (frequency between 0.01 and 0.1 Hz) during episodic storms has been shown to cause larger microseismic ground displacements, in the order of a few µm, exceeding the damage threshold of the rock mass and causing microcrack propagation and coalescence that will prepare rock fracturing and collapse (Brain et al., 2014). Whereas Brain et al. (2014) express however doubts about such storm wave loading being a significant cause of mass movement and believe it might at best contribute to rock strength decrease if rocks have been submitted to pre-damaged conditions by other factors, Earlie et al. (2015) measured microseismic ground movements one to two orders of magnitude higher (50–100 µm) during the extreme storm event of January 31 to February 6, 2014 on top of 8–10 m high cliffs exposing Devonian slates along the coasts of SW England. They were able to link these motions directly to video capture of large wave impacts, wave overtopping and small-scale cliff collapse events, which amounted to 1350 m^3 of eroded material from a 300 m long cliff section over the 2 week long storm period, thus demonstrating the effectiveness of dynamic loading by extreme storm waves as a trigger of cliff failure (Fig. 6). Empirical evidence collected by Bezzera et al. (2011) along the sea cliffs of Central

Algarve, Portugal, further confirmed the finding of Earlie et al. (2015). Indeed, looking at mass movements recorded in five sectors of the coast where cliffs are cut into Miocene carbonate rocks, they identified a strong correlation ($r = 0.89$) between the energy of the storm waves hitting the cliffs with a 10-year return period and total volumes of landslides.

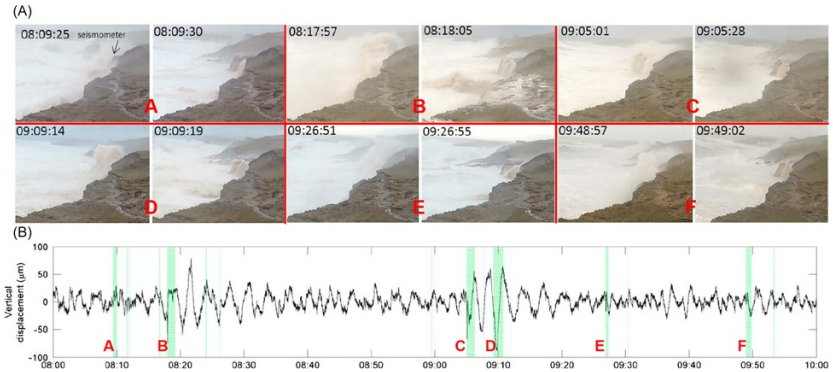

Fig. 6 Porthleven, SW Cornwall (United Kingdom), February 5, 2014, during the largest Atlantic storm since at least the 1950s. Microseismic ground movements measured on the flat top of a cliff (B; see the seismometer location on the first video capture) in relation with successive wave overtopping and subsequent drainage events (A; pairs of successive images). Green bands in the ground motion time series correspond to the phases of water cascading down the cliff face.

From Earlie C, Young A, Masselink G and Russell P (2015) Coastal cliff ground motions and response to extreme storm waves. Geophysical Research Letters 42: 847–854, doi:10.1002/2014GL062534.

alt-text: Fig. 6

3.7 (Local) overloading by fills and heavy constructions

The great variety of artificial loads that can threaten the stability of slopes and the engineering issues they involve constitute a vast research field on its own, which is out of the scope of this article. Therefore, we only provide key information on the types and characteristics of such added loads and the settings in which they may impact slope stability, as it will be illustrated by a few examples.

Anthropogenic loading of slopes by construction comprises point loads of, e.g., bridge piles or towers involving highly concentrated local stresses (including water towers sometimes located close to the top of slopes); more distributed loads created by individual buildings of every size, shape, height and weight; line loads associated with slope cut-and-fill for, e.g., road construction; and quasi-uniform loading of entire hillsides invaded by the suburban development of megacities. Another type of human-induced loading frequently responsible of landslides results from the huge amounts of waste produced by the modern societies, with volumes of individual accumulations reaching many millions of cubic meters and representing enormous loads that either may threaten the stability of the slopes on which they are deposited or become themselves hazardous by failure of their own artificial slopes. Municipal and construction waste (hereafter MSW and CSW for municipal and construction solid waste, respectively) involve different settings of solid waste landfill with specific mechanical properties requiring different engineering treatments. Beside waste, voluminous landfill is also more and more involved in construction works, e.g., for highway or railway embankments. Finally, anthropogenic loading eventually leading to unexpected slope failure may also be caused by water accumulating in the slope material due to leakage or burst of pipes and septic tanks, or infiltration from canals, or intensive irrigation of cropland, with the common twofold impact on slopes of added weight and increased pore pressure (e.g., Kazmi et al., 2017).

The following numbers highlight the potential impact of loading of slopes by human activities. With respect to point loads, a typical 2000 m^3 water tower imposes for example a total load (weight of the structure + reservoir content) in the order of 60 MN on its supporting reinforced concrete slab, however generally transmitted to firm layers at depth by anchoring concrete piles. As for highway bridge piles, the recommended value of allowable bearing pressure for their spread footing foundations is for instance 1.92 MPa on hard sound sedimentary rocks (AASHTO, 2002). By contrast, buildings mostly develop much lower loads. Engineers distinguish the dead load of a building, i.e., the load of its structure (foundations, walls, floors, roof) and its live load comprised of furniture, people, cars, snow or rain, etc. As an example, Keersmaeckers et al. (2005) mention a total (gravity) load of apartment buildings in the order of 10 kPa per story. Live loads depend on the use of the building, with (uniformly distributed) design live load intensities fixed by the American Society of Civil Engineers at, e.g., 1.92 kPa for passenger car parking garages and habitable rooms of a family dwelling, 4.79 kPa for a restaurant floor, or 11.97 kPa for heavy manufacturing plants (ASCE, 2010). However, average realized live loads (Dunham et al., 1952) are generally less than half the design loads. Compared to the ASCE (2010) design norm of 7.18 kPa for library stack rooms, Tapia-Hernández et al. (2019) measured for example actual live loads (comprised of shelves, books, and standing people) of 3.5 kPa on average in a public library in Mexico City. Though being rarely itself the trigger of landsliding, slope (over)loading by buildings may become an issue especially in rapidly growing urban settings where hillsides are overcrowded with wild housing or poorly engineered apartment buildings, and it is regularly mentioned as one among several anthropogenic hazard-enhancing factors especially for rainfall-triggered landslides affecting densely constructed steep slopes of intertropical cities

(Jones, 1973; Smyth and Royle, 2000). It should also be stressed that part of the problem is related to the fact that in most small- and medium-scale especially residential or commercial construction projects, loading issues and possible remedial measures are envisaged in terms of settlement and stability of the building much more than stability of the supporting slope.

Unsurprisingly, the diversity of anthropogenic load types entails a variety of ways these loads impact slope stability, with permanent (dead) and transient (part of live) loads, time-dependent loads of growing waste dumps, the dynamic load component of traffic vibrations transmitted to the ground by highway piles or train vibrations affecting railway embankments (e.g., Jongmans et al., 1999). In the case of rapid landfilling associated with large construction works or waste management, the initial loading impact is transiently high (for up to a few years) due to increased pore pressure under undrained-equivalent conditions, until it gradually decreases when drained conditions progressively reestablish (e.g., Hsi and Martin, 2015). The case of the December 2015 CSW landfill failure at Shenzhen, China, with a $2.73 \times 10^6\,m^3$ failed volume and 77 killed people, involved however a more complex set of causes (Yin et al., 2016) (Fig. 7). Filling an abandoned open pit, the CSW was first deposited at the downslope entrance of the excavation, with consolidation and terracing of its outer slope and continued filling on the inner slope, which caused rain and water percolating from the CSW to pond in the bottom of the pit, at lower elevation than the CSW accumulation. The failure occurred ~~i~~on December 20, 2015, after about 1 million m^3 CSW landfill had been added within ~ 8 months. Saturation of the poorly consolidated pit bottom material by infiltrating surface water (aggravated by deficiencies in the drainage system), and consolidation seepage and gradual elevation of the level of water infiltration due to the continuously growing CSW accumulation combined to increase the pore pressure head in the front slope, eventually leading to excess pore pressure and slope failure.

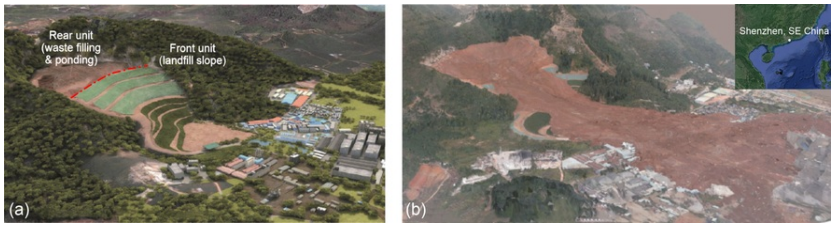

Fig. 7 Failure of a large CSW landfill in progress at Shenzhen, China, on December 20, 2015. With a 2.73 $10^6\,m^3$ slid volume, the landslide destroyed 33 buildings and killed 77 people. It resulted from a complex set of causes in which overloading played a key role. (A) The landfill in progress 2 days before the landslide, with the terraced front slope and the not yet filled ponding area at the rear of the fill, separated by the red axis line. (B) Aerial view of the landslide 1 day after the event.
Modified from Yin Y, Li B, Wang W, Zhan L, Xue Q, Gao Y, Zhang N, Chen H, Liu T and Li A (2016) Mechanism of the December 2015 catastrophic landslide at the Shenzhen landfill and controlling geotechnical risks of urbanization. Engineering 2: 230–249.

alt-text: Fig. 7

In uncontrolled or poorly engineered MSW dumps, the load increase with increasing height of uncompacted or inconsistently compacted waste is known to have caused several slope failures, sometimes through static liquefaction and often causing large numbers of fatalities in less developed settings (Blight, 2008). However, even in well monitored MSW dumps may accidents occur. On March 9, 1996, a slope failure involving about $1.2 \times 10^6\,m^3$ of waste affected a MSW landfill near Cincinnati, Ohio (Stark et al., 2000). Although a 1994 permit for lateral expansion of the MSW, which required creating a new excavation, had allowed in the same time a 7.5-m increase of the waste fill elevation, the latter was already by 1996 15 m higher than permitted, with an overfill volume of $\sim 0.78 \times 10^6\,m^3$ of the slope that was to fail. The basal failure surface developed within the native brown soil between the waste and the bedrock shales, with first slide motions starting in the slope toe toward the expansion excavation and propagating rapidly in the entire slope. Slope overbuild, involving excessive load and increased slope gradient, and strain incompatibility between the MSW and the underlying native soil were identified as the major factors responsible for this slope failure, whose eventual trigger was rock blasting in the adjacent excavation (Stark et al., 2000).

As a concluding example, let's finally evoke the causes of the submarine landslide that occurred on November 3, 1994, at Skagway, Alaska (Cornforth, 2005) (Fig. 8). The landslide destroyed a length of ~ 250 m of timber docks and ~ 50 m of sheetpile cellular structure of newly built docks along the steep rocky side of the fjord in which Skagway harbor lies. The equally steep underwater talus of the rocky cliff is overlain by up to ~ 25 m marine silts. Before the accident, there existed only a narrow embankment supporting a railway track at the foot of the hillside, the old timber docks being constructed ~ 15 m from the shore. Prior to the start of the new dock construction, the gap between old docks and shore was filled with soil and rock in order to gain space and stockpile riprap, corresponding to a total volume of $\sim 10.5 \times 10^3\,m^3$ of material added just south of the construction area. Slope failure occurred during the construction works, after filling of the fourth of the planned 23 cells of the new docks, when an extreme low tide removed every water buttress of the piles. Scour contours suggest the flow slide volume was $\sim 0.9 \times 10^6\,m^3$ immediately below the dock, but a much larger volume of material was mobilized down to the bottom of the bay. This submarine slide in turn triggered a tsunami wave up to 9–11 m in height at the shoreline and 5–6 m in the Skagway harbor, causing significant damage to the ferry terminal (Kulikov et al., 1996). In such a case, it is evident that loading of the upper talus slope by fill plus riprap, with a total estimated weight of 22.5×10^3 tons, is the chief trigger of the initial shear slide and the subsequent major flow slide under the specific circumstances of extreme low tide. Stability analyses showed that such an added load decreased the factor of safety of the shallow upper part of the slope by 0.3, bringing it around 1.0 at very low tide (Cornforth, 2005). Moreover, post-failure investigations showed that most sheetpiles had not reached hard bedrock, being only driven within the cohesionless soft marine mud. Therefore, ~~what~~however inescapable the triggering effect of overloading may have been, the true cause of this landslide must be searched in a human lack of foresight.

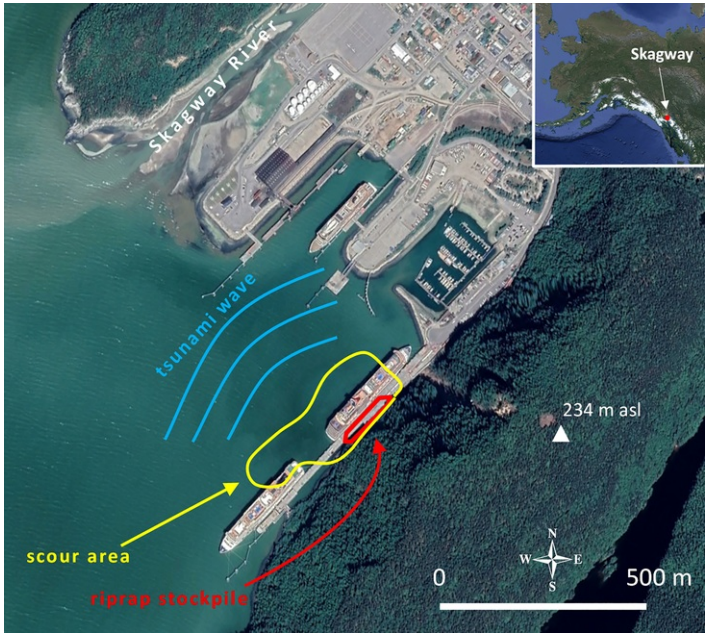

Fig. 8 Location and main characteristics of the overloading-triggered submarine landslide and subsequent tsunami at Skagway (SE Alaska) on November 3, 1994. The fill behind the pre-1994 wood wharf was overloaded by riprap stockpiling (area in red). In yellow, the scour area of the slide (Cornforth, 2005).

Image 14.12.2015: © Google Earth.

alt-text: Fig. 8

References

AASHTO (American Association of State Highway and Transportation Officials), Standard Specifications for Highway Bridges, 17th edn, 2002, AASHTO, Washington, DC, 20001, 829 + 137 (commentaries) p.

Abernethy B. and Rutherfurd I., Does the weight of riparian trees destabilize riverbanks?, *Regulated Rivers Research & Management* **16**, 2000, 565–576.

Adams P., Storlazzi P. and Anderson R., Nearshore wave-induced cyclical flexing of sea cliffs, *Journal of Geophysical Research* **110**, 2005, F02002, https://doi.org/10.1029/2004JF000217.

Ancey C., Snow avalanches, In: Balmforth N. and Provenzale A., (Eds.), *Geomorphological Fluid Mechanics, Lecture Notes in Physics* **vol. 582**, 2001, Springer, 319–338.

Arias A., A measure of earthquake intensity, In: Hansen R., (Ed), *Seismic Design for Nuclear Power Plants,* 1970, MIT Press, Cambridge, MA, 438–483.

ASCE (American Society of Civil Engineers), Minimum design loads for buildings and other structures, In: *ASCE Standards ASCE/SEI 7-10,* 2010, ASCE, Reston, VA, 605 p.

Ashford S., Sitar N., Lysmer J. and Deng N., Topographic effects on the seismic response of steep slopes, *Bulletin of the Seismological Society of America* **87** (3), 1997, 701–709.

Ashland F., Characteristics, Causes, and Implications of the 1998 Wasatch Front landslides, 2003, Utah Geological Survey, Utah, ~~49,~~ Special Study 105, 49 p.

Bezzera M., Moura D., Ferreira O. and Taborda R., Influence of wave action and lithology on sea cliff mass movements in Central Algarve Coast, Portugal, *Journal of Coastal Research* **27** (6A), 2011, 162–171.

Blight G., Slope failures in municipal solid waste dumps and landfills: A review, *Waste Management & Research* **26**, 2008, 448–463.

Brain M., Rosser N., Norman E. and Petley D., Are microseismic ground displacements a significant geomorphic agent?, *Geomorphology* **207**, 2014, 161–173.

Brain M., Rosser N., Sutton J., Snelling K., Tunstall N. and Petley D., The effects of normal and shear stress wave phasing on coseismic landslide displacement, *Journal of Geophysical Research - Earth Surface* **120**, 2015, 1009–1022.

Bray J. and Travasarou T., Simplified procedure for estimating earthquake-induced deviatoric slope displacements, *Journal of Geotechnical and Geoenvironmental Engineering, ASCE* **133** (4), 2007, 381–392.

Bray J. and Travasarou T., Pseudostatic coefficient for use in simplified seismic slope stability evaluation, *Journal of Geotechnical and Geoenvironmental Engineering, ASCE* **135** (9), 2009, 1336–1340.

Bray J. and Travasarou T., Pseudostatic slope stability procedure, In: Proceedings 5th International Conference on Earthquake Geotechnical Engineering, 5ICEGE, Santiago, Chile, Theme Lecture 1, 10–13 January, 2011, , 2011, 12 p.

Broeckx J., Rossi M., Lijnen K., Campforts B., Poesen J. and Vanmaercke M., Landslide mobilization rates: A global analysis and model, *Earth-Science Reviews* **201**, 2020, , (the second comma must be deleted.)102972, https://doi.org/10.1016/j.earscirev.2019.102972.

Calcaterra D. and Parise M., Weathering as a Predisposing Factor to Slope Movements, *Engineering Geology Special Publications* 2010, Bath Geological Society, 245.

Chen Z., Mi H., Zhang F. and Wang X., A simplified method for 3D slope stability analysis, *Canadian Geotechnical Journal* **40**, 2003, 675–683.

Cheng Y., Lansivaara T. and Wei W., Two-dimensional slope stability analysis by limit equilibrium and strength reduction methods, *Computers and Geotechnics* **34**, 2007, 137–150.

Cheng Y., Li N. and Yang X., Three-dimensional slope stability problem with a surcharge load, *Natural Hazards and Earth System Sciences* **15**, 2015, 2227–2240.

Chiaradia E., Vergani C. and Bischetti G., Evaluation of the effects of three European forest types on slope stability by field and probabilistic analyses and their implications for forest management, *Forest Ecology and Management* **370**, 2016, 114–129.

Coder K., Tree Anchorage and Root Strength, 2014, University of Georgia; Warnell School of Forestry and Natural Resources Monograph Publication WSFNR14-9, 67 p.

Collins B. and Sitar N., Processes of coastal bluff erosion in weakly lithified sands, Pacifica, California, USA, *Geomorphology* **97**, 2008, 483–501.

Cornforth D., Landslides in Practice, 2005, Wiley, 596 p.

Cummings D., Boone Kauffman J., Perry D. and Hughes R., Aboveground biomass and structure of rainforests in the southwestern Brazilian Amazon, *Forest Ecology and Management* **163**, 2002, 293–307.

Demoulin A. and Glade T., Recent landslide activity in Manaihan, East Belgium, *Landslides* **1**, 2004, 305–310, https://doi.org/10.1007/s10346-004-0035-z.

Dunham J., Brekke G. and Thompson G., Live loads on floors in buildings, In: *Building Materials and Structures Report,* **vol. 133**, 1952, US Department of Commerce, National Bureau of Standards, 27 p.

Durgin P., Landslides and the Weathering of Granitic Rocks, *Reviews in Engineering Geology* **vol. III**, 1977, Geological Society of America, 127–131.

Earlie C., Young A., Masselink G. and Russell P., Coastal cliff ground motions and response to extreme storm waves, *Geophysical Research Letters* **42**, 2015, 847–854, https://doi.org/10.1002/2014GL062534.

Ekayanake J., Marden M., Watson A. and Rowan D., Tree roots and slope stability: A comparison between *Pinus radiata* and Kānuka, *New Zealand Journal of Forestry Science* **27** (2), 1997, 216–233.

El-Ramly H., Morgenstern R. and Cruden D., Probabilistic slope stability analysis for practice, *Canadian Geotechnical Journal* **39**, 2002, 665–683.

Fan X., Xu Q., Scaringi G., Dai L., Li W., Dong X., Zhu X., Pei X., Dai K. and Havenith H.B., Failure mechanism and kinematics of the deadly June 24th 2017 Xinmo landslide, Maoxian, Sichuan, China, *Landslides* **14**, 2017, 2129–2146, https://doi.org/10.1007/s10346-017-0907-7.

Fayolle A., Doucet J.L., Gillet J.F., Bourland N. and Lejeune P., Tree allometry in Central Africa: Testing the validity of pantropical multi-species allometric equations for estimating biomass and carbon stocks, *Forest Ecology and Management* **305**, 2013, 29–37.

Fellenius W., Erdstatische Berechnungen mit Reibung und Kohäsion (Adhäsion) und unter Annahme kreiszylindrischer Gleitflächen, 1927, W. Ernst & Sohn, Berlin, 40 p.

Fleming R., Johnson R. and Schuster R., The reactivation of the Manti landslide, Utah, In: USGS Professional Paper 1311, The Manti, Utah, Landslide, 1988, 1–22.

Froude M. and Petley D., Global fatal landslide occurrence from 2004 to 2016, *Natural Hazards and Earth System Sciences* **18**, 2018, 2161–2181, https://doi.org/10.5194/nhess-18-2161-2018.

Garcia-Mayordomo J., Rodriguez Peces M., Azañon J. and Insua Arévalo J., Advances and trends on earthquake-triggered landslide research in Spain, In: Proceeding of the 1st INQUA-IGCP-567 International Workshop on Earthquake Archaeology and Palaeoseismology, Baelo Claudia, Spain, 7–13 September 2009, 2009, 28–31.

Garcia-Rodriguez M., Havenith H. and Benito B., Evaluation of earthquake-triggered landslides in El Salvador using a GIS-based Newmark model, In: Proceeding of the 14th World Conference on Earthquake Engineering, October 12–17, 2008, Beijing, China, 2008.

Geertsema M., Quick clay, In: Bobrowsky P., (Ed), *Encyclopedia of Natural Hazards,* 2013, Springer, 803–804.

Genet M., Stokes A., Fourcaud T. and Norris J., The influence of plant diversity on slope stability in a moist evergreen deciduous forest, *Ecological Engineering* **36** (3), 2010, 265–275.

Gerolymos N., Numerical modeling of seismic triggering, evolution, and deposition of rapid landslides: Application to Higashi-Takezawa (2004), *International Journal for Numerical and Analytical Methods in Geomechanics* **34**, 2010, 383–407.

Gonzalez de Tanago J., Lau A., Bartholomeus H., Herold M., Avitabile V., Raumonen P., Martius C., Goodman R., Disney M., Manuri S., Burt A. and Calders C., Estimation of above-ground biomass of large tropical trees with terrestrial LiDAR, *Methods in Ecology and Evolution* **9**, 2018, 223–234.

Gray D., Role of woody vegetation in reinforcing soils and stabilising slopes, In: Proceeding of the Symposium Soil Reinforcing and Stabilising Techniques, Sydney, Australia, 1978, 253–306.

Gray D. and Megahan W., Forest Vegetation Removal and Slope Stability in the Idaho Batholith, USDA, Research Paper INT-271: Ogden, Utah. 1981, 23 p.

Greenway D., Vegetation and slope stability, In: Anderson M. and Richards K., (Eds.), *Slope Stability, Geotechnical Engineering and Geomorphology* 1987, Wiley, 187–230.

Gregersen O., The quick clay landslide in Rissa, Norway, In: Proceeding of the 10th International Conference on Soil Mechanics and Foundation Engineering, Stockholm, 15–19 June 1981, Balkema, Rotterdam, 1981, 421–426.

Griffiths D. and Lane P., Slope stability analysis by finite elements, *Geotechnique* **49** (3), 1999, 387–403.

Hammond C., Hall D., Miller S. and Swetik P., Level I Stability Analyses (LISA) Documentation for Version 2.0, USDA, General Technical Reports INT-285: Ogden, Utah. 1992, 190 p.

Hao L., Huang F., Liu Y. and Li L., Avalanche activity and characteristics of its triggering factors in the western Tianshan Mountains, China, *Journal of Mountain Science* **15** (7), 2018, 1397–1411.

Higuchi N., dos Santos J., Imanaga M. and Yoshida S., Aboveground biomass estimate for Amazonian dense tropical moist forests, *Memoirs of the Faculty of Agriculture, Kagoshima University* **30**, 1994, 43–54.

His J. and Martin J., Soft ground treatment and performance, Yelgun to Chinderah Freeway, New South Wales, Australia, In: Indraratna B., Chu J. and Rujikiatkamjorn C., (Eds.), *Ground Improvement Case Histories, Compaction, Grouting and Geosynthetics*, 2015, Elsevier, 137–174.

Hsieh S. and Lee C., Empirical estimation of the Newmark displacement from the Arias intensity and critical acceleration, *Engineering Geology* **122**, 2011, 34–42.

Huang C. and Tsai C., New method for 3D and asymmetrical slope stability analysis, *Journal of Geotechnical and Geoenviromental Engineering* **126** (10), 2000, 917–927.

Huang D., Song Y., Cen D. and Fu G., Numerical modeling of earthquake-induced landslide using an improved discontinuous deformation analysis considering dynamic friction degradation of joints, *Rock Mechanics and Rock Engineering* **49**, 2016, 4767–4786.

Hutchinson J., Assessment of the effectiveness of corrective measures in relation to geological conditions and types of slope movement, *Bulletin International Association of Engineering Geologists* **16**, 1977, 131–155.

Hutchinson J., An influence line approach to the stabilization of slopes by cuts and fills, *Canadian Geotechnical Journal* **21**, 1984, 363–370.

Hynes-Griffin M. and Franklin A., Rationalizing the Seismic Coefficient Method, Miscellaneous Paper GL-84-13. 1984, US Army Engineer WES, Vicksburg, MS, 21 p., + annexes.

Ingles J., Darrozes J. and Soula J.C., Effects of the vertical component of ground shaking on earthquake-induced landslide displacements using generalized Newmark analysis, *Engineering Geology* **86**, 2006, 134–147.

Ioki K., Tsuyuki S., Hirata Y., Phua M., Wong W., Ling Z., Saito H. and Takao G., Estimating above-ground biomass of tropical rainforest of different degradation levels in Northern Borneo using airborne LiDAR, *Forest Ecology and Management* **328**, 2014, 335–341.

Iverson R., Sensitivity of stability analyses to groundwater data, In: Bell D., (Ed), Proceedings of the Sixth International Symposium on Landslides, Balkema, 1991, 451–457.

Ji J., Kokutse N., Genet M., Fourcaud T. and Zhang Z., Effect of spatial variation of tree root characteristics on slope stability. A case study on Black locust (*Robinia pseudoacacia*) and Arborvitae (*Platycladus orientalis*) stands on the loess Plateau, China, *Catena* **92**, 2012, 139–154.

Jibson R., Predicting earthquake-induced landslide displacements using Newmark's sliding block analysis, *Transportation Research Record* **1411**, 1993, 9–17.

Jibson R., Regression models for estimating coseismic landslide displacement, *Engineering Geology* **91**, 2007, 209–218.

Jibson R. and Keefer D., Analysis of the seismic origin of landslides: Examples from the New Madrid seismic zone, *Geological Society of America Bulletin* **105**, 1993, 521–536.

Jibson R., Harp E. and Michael J., A Method for Producing Digital Probabilistic Seismic Landslide Hazard Maps: An Example From the Los Angeles, California, Area, US Geological Survey Open-File Report 98-113. 1998, 17 p.

Johansson T., Biomass production of Norway spruce (*Picea abies* (L.) Karst.) growing on abandoned farmland, *Silva Fennica* **33** (4), 1999, 261–280.

Jones F., Landslides of Rio de Janeiro and the Serra das Araras Escarpment, Brazil, U.S. Geological Survey Professional Paper 697. 1973, 42 p.

Jongmans D., Demanet D., Havenith H. and Hemroulle P., Application of 2D electrical and seismic tomography techniques for investigating landslide sites, In: Abstracts of the 5th EEGS-ES Meeting, Budapest, Hungary, September 6–9, 1999, EAGE Publications, LS-03, 1999, 2 p.

Kab A., Djerbal L. and Bahar R., Landslide susceptibility mapping of Tizi-Ouzou region, Algeria, In: Wasowski J., Giordan D. and Lollino P., (Eds.), *Engineering Geology and Geological Engineering for Sustainable Use of the Earth's Resources, Urbanization and Infrastructure Protection From Geohazards,* 2018, Springer International Publishing AG, 140–148.

Kazmi D., Qasim S., Harahap I. and Vu T., Analytical study of the causes of the major landslide of Bujit Antarabangsa in 2008 using fault tree analysis, *Innovative Infrastructure Solutions* **2**, 2017, 55, https://doi.org/10.1007/s41062-017-0105-4.

Keefer D., Landslides caused by earthquakes, *Geological Society of America Bulletin* **95**, 1984, 406–421.

Keefer D. and Wilson R., Predicting earthquake-induced landslides, with emphasis on arid and semi-arid environments, In: Sadler P. and Morton D., (Eds.), *Landslides in a Semi-Arid Environment,* **vol. 2**, 1989, Inland Geological Society, Riverside, CA, 118–149.

Keersmaeckers R., Maertens J. and Van Gemert D., ~~(2005)~~ Verkennende ~~S~~studie ~~M~~met ~~B~~betrekking ~~T~~tot ~~M~~massabewegingen in de Vlaamse Ardennen. Deel II: Geotechnisch ~~O~~onderzoek van ~~E~~enkele ~~R~~representatieve ~~S~~sites ~~O~~onderhevig aan ~~M~~massabewegingen. Report Laboratorium Reyntjens R/30232/04~~.~~, 2005, Report Commissioned by the Vlaamse Gemeenschap, AMINAL, Afdeling Land, ~~p.~~ 154 p.

Kim D., Im S., Lee C. and Woo C., Modeling the contribution of trees to shallow landslide development in a steep, forested watershed, *Ecological Engineering* **61P**, 2013, 658–668.

Krahn J., The 2001 R.M. Hardy lecture: The limits of limit equilibrium analyses, *Canadian Geotechnical Journal* **40**, 2003, 643–660.

Kulikov E., Rabinovich A., Thomson R. and Bornhold B., The landslide tsunami of November 3, 1994, Skagway Harbor, Alaska, *Journal of Geophysical Research* **101** (C3), 1996, 6609–6615.

Laws M. and Murray J., Impacts of poor urban land development on slope instability, In: Geohazard Conference 2011, Kelowna, British Columbia, Canada, 2011, 8 p.

Lewis S., et al., Above-ground biomass and structure of 260 African tropical forests, *Philosophical Transactions of the Royal Society B* **368**, 2013, , (delete the second comma)20120295, https://doi.org/10.1098/rstb.2012.0295.

L'Heureux J., Eilertsen R., Glimsdal E., Issler D., Solberg I. and Harbitz C., The 1978 quick clay landslide at Rissa, Mid Norway: Subaqueous morphology and tsunami simulations, In: Yamada Y., et al., (Eds.), *Submarine Mass Movements and Their Consequences, Advances in Natural and Technological Hazards Research* **vol. 31**, 2012, Springer, 507–516.

Ma S. and Xu C., Applicability of two Newmark models in the assessment of coseismic landslide hazard and estimation of slope-failure probability: An example of the 2008 Wenchuan M_w 7.9 earthquake affected area, *Journal of Earth Science* **30** (5), 2019, 1020–1030.

Maffra C., Sousa R., Sutili F. and Pinheiro R., The effect of roots on the shear strength of texturally distinct soils, *Floresta e Ambiente* **26** (3), 2019, , (delete the second comma)e20171018, https://doi.org/10.1590/2179 8087.101817.

Martin C., Morley A. and Griffiths J., Introduction to engineering geology and geomorphology of glaciated and periglaciated terrains, In: Griffiths J. and Martin C., (Eds.), *Engineering Geology and Geomorphology of Glaciated and Periglaciated Terrains—Engineering Group Working Party Report,* **vol. 28**, 2017, Geological Society, London, 1–30, Engineering Geology Special Publications, **vol. 28**, 2017, 1–30.

Matsui T. and San K., Finite element slope stability analysis by shear strength reduction technique, *Soils and Foundations* **32** (1), 1992, 59–70.

Mulder H., Assessment of Landslide Hazard, PhD thesis. 1991, Utrecht University, Utrecht, 149p.

Nadim F., Høydal Ø., Haugland H. and McLean A., Analysis of Landslides Triggered by Anthropogenic Factors in Europe, 2011, Deliverable D1.6. SafeLand—FP7, Grant Agreement 226479, 82 p.

Naylor D., Finite elements and slope stability, Numerical methods, In: Geomechanics, Proceedings of the NATO Advanced Study Institute, Lisbon, 1981, 229–244.

Newmark N., Effects of earthquakes on dams and embankments, *Geotechnique* **15** (2), 1965, 139–160.

Sanquetta C., Corte A. and da Silva F., Biomass expansion factor and root-to-shoot ratio for Pinus in Brazil, *Carbon Balance and Management* **6**, 2011, 6.

Sazzad M. and Haque M., Effect of surcharge on the stability of slope in a homogeneous soil by FEM, In: *Proceeding of the 2nd International Conference on Advances in Civil Engineering, 26–28 December, 2014 CUET, Chittagong, Bangladesh,* 2014, 314–318.

Schwarz M., Cohen D. and Or D., Spatial characterization of root reinforcement at stand scale: Theory and case study, *Geomorphology* **171–172**, 2012, 190–200.

Seed H., Considerations in the earthquake-resistant design of earth and rockfill dams, *Geotechnique* **29** (3), 1979, 215–263.

Selby M., Hillslope Materials and Processes, 2nd edn, 1993, Oxford University Press, Oxford, 451 p.

Simon A. and Collison A., Quantifying the mechanical and hydrologic effects of riparian vegetation on streambank stability, *Earth Surface Processes and Landforms* **27**, 2002, 527–546.

Smyth C. and Royle S., Urban landslide hazards: Incidence and causative factors in Niterói, Rio de Janeiro State, Brazil, *Applied Geography* **20**, 2000, 95–117.

Speight J. and Isbell R., Substrate, The National Committee on Soil and Terrain (Ed.). In: *Australian Soil and Land Survey Field Handbook,* 2009, CSIRO, 201–224.

Stark T., Eid H., Evans W. and Sherry P., Municipal solid waste slope failure II: Stability analyses, *Journal of Geotechnical and Geoenviromental Engineering* **126** (5), 2000, 408–419.

Su L., Hu K., Zhang W., Wang J., Lei Y., Zhang C., Cui P., Pasuto A. and Zheng Q., Characteristics and triggering mechanism of Xinmo landslide on 24 June 2017 in Sichuan, China, *Journal of Mountain Science* **14** (9), 2017 1689–1700.

Sun G., Ranson K., Guo Z., Zhang Z., Montesano P. and Kimes D., Forest biomass mapping from lidar and radar synergies, *Remote Sensing of Environment* **115**, 2011, 2906–2916.

Szwagrzyk J. and Gazda A., Above-ground standing biomass and tree species diversity in natural stands of Central Europe, *Journal of Vegetation Science* **18**, 2007, 555–562.

Tapia-Hernández E., Dominguez-Palacios A. and Martinez-Ruiz M., Live loads on floors of libraries and newspaper archive buildings, *International Journal of Advanced Structural Engineering* **11**, 2019, 285–296.

Terzaghi K., Critical height and factor of safety of slopes against sliding, In: Proceeding of the International Conference on Soil Mechanics and Foundation Engineering, Cambridge, MA, **vol. 1**, 1936, 156–161.

Torgoev A., Havenith H.B. and Lamair L., Improvement of seismic landslide susceptibility assessment through consideration of geological and topographic amplifications factors, In: Troisièmes Journées Aléas Gravitaires, Grenoble, France, 17–18 Septembre 2013, 2013, 6 p.

Torrance J., Landslides in quick clay, In: Clague J. and Stead D., (Eds.), *Landslides: Types, Mechanisms and Modeling,* 2012, Cambridge University Press, 83–94.

Van Asch T., Deimel M., Haak W. and Simon J., The viscous creep component in shallow clayey soil and the influence of tree load on creep rates, *Earth Surface Processes and Landforms* **14**, 1989, 557–564.

Van den Eeckhaut M, Poesen J, Hervás J (2013) Mass-movement causes: Overloading. In: Shroder J (Editor in Chief), Marston R and Stoffel M (Eds), Treatise on Geomorphology, Academic Press: San Diego, CA, vol. 7, Mountain and Hillslope Geomorphology, 1st edn, pp. 200-206.

Wakai A., Ugai K., Onoue A., Kuroda S. and Higuchi K., Numerical modeling of an earthquake-induced landslide considering the strain-softening characteristics at the bedding plane, *Soils and Foundations* **50** (4), 2010, 533–545.

Wan Y., Gao Y. and Zhang F., A simplified approach to determine the unique direction of sliding in 3D slopes, *Engineering Geology* **211**, 2016, 179–183.

Wan Y., Gao Y. and Zhang F., Stability analysis of three-dimensional slopes considering the earthquake force direction, *Mathematical Problems in Engineering* 2018, https://doi.org/10.1155/2018/2381370.

Wang Y., Zhao B. and Li J., Mechanism of the catastrophic June 2017 landslide at Xinmo Village, Songping River, Sichuan Province, China, *Landslides* **15**, 2018, 333–345, https://doi.org/10.1007/s10346-017-0927-3.

Ward T., Factor of Safety Approach to Landslide Potential Delineation, PhD Thesis. 1976, Colorado State University, Fort Collins, 128 p.

Wieczorek G., Landslide triggering mechanisms, In: Turner A. and Schuster R., (Eds.), *Landslides,* 1996, 76–90, Inverstigation and Mitigation, Special Report 247, Transportation Research Board, NRC.

Wieczorek G., Wilson R. and Harp E., Map Showing Slope Stability During Earthquakes of San Mateo County, California, 1985, US Geological Survey, Miscellaneous Geologic Investigations Map I-1257-E, scale 1:62,500.

Wilson R., Relation of Arias Intensity to Magnitude and Distance in California, 1993, US Geological Survey, 42, Open-File Report 93-556, 42 p.

Wilson R. and Keefer D., Predicting areal limits of earthquake-induced landsliding, In: Ziony J., (Ed), *Earthquake Hazards in the Los Angeles Metropolitan Area,* 1985, US Geological Survey, 317–345, Professional Paper 1360.

Wolters G. and Müller G., The propagation of wave impact induced pressures into cracks and fissures, In: Mortimore R. and Duperret A., (Eds.), *Coastal Chalk Cliff Instability,* **vol. 20**, 2004, Geological Society, London, 121–130, Engineering Geology Special Publications, **vol. 20**, 2004, 121–130.

Wu T., McKinnell W. and Swanston D., Strength of tree roots and landslides on Prince of Wales Island, Alaska, *Canadian Geotechnical Journal* **16**, 1979, 19–33.

Xu L., Saatchi S., Shapiro A., Meyer V., Ferraz A., Yang Y., Bastin J.F., Banks N., Boeckx P., Verbeeck H., Lewis S., Muanza E., Bongwele E., Kayembe F., Mbenza D., Kalau L., Mukendi F., Ilunga F. and Ebuta D., Spatial distribution of carbon stored in forests of the Democratic Republic of Congo, *Scientific Reports* **7**, 2017, 15030, https://doi.org/10.1038/s41598-017-15050-z.

Yamakura T., Hagihara A., Sukardjo S. and Ogawa H., Aboveground biomass of tropical rain forest stands in Indonesian Borneo, *Vegetatio* **68**, 1986, 71–82.

Yang X., Yang G. and Yu T., Comparison of strength reduction method for slope stability analysis based on ABAQUS FEM and FLAC^{3D} FDM, *Applied Mechanics and Materials* **170–173**, 2012, 918–922.

Yin Y., Li B., Wang W., Zhan L., Xue Q., Gao Y., Zhang N., Chen H., Liu T. and Li A., Mechanism of the December 2015 catastrophic landslide at the Shenzhen landfill and controlling geotechnical risks of urbanization, *Engineering* **2**, 2016, 230–249.

Ziemer R., Roots and the stability of forested slopes, In: *Erosion and Sediment Transport in Pacific Rim Steeplands,* **132**, 1981, IAHS Publishing, Christchurch, 343–361.

Zienkiewicz O., Humpheson C. and Lewis R., Associated and non-associated visco-plasticity and plasticity in soil mechanics, *Geotechnique* **25** (4), 1975, 671–689.

Abstract

Overloading is defined as the addition onto a slope of excessive surcharge load, which either directly triggers landsliding or brings the slope so close to failure that any small accidental trigger will imminentl cause it to fail. Static surcharge loading may occur in various natural settings under the weight of groundwater, growing forest, volcanic fallout, displaced soil or rock masses, but is now also more and more frequentl related to human activities concerned with large construction works, solid waste disposal, and urban development on steep slopes. Dynamic loading may be considered another kind of transient surcharge, broadenin the scope of overloading issues to earthquake-triggered landslides, coastal cliff collapse under extreme storm wave action, and human-induced dynamic loading, e.g., from traffic vibrations or mine blasting. Howeve although (over)loading is undoubtedly involved in many mass-movement events, its definite contribution to the rupture process remains often elusive. This is either because, as a primary driver, it is more or les overshadowed by a more apparent trigger, such as the loss of strength caused by pore pressure increase, or it acts as part of an intricate set of causative factors, which is for instance the case when tree loadin interferes with vegetation-dependent changes in pore pressure and the effect of the root mat on soil cohesion. The difficulty in assessing the influence of a surcharge load derives also from its twofold effect c simultaneously altering the slip driving and resisting forces, which stresses the importance of slope gradient for modulating its net impact on stability. Examination of the theoretical changes brought by an added loa to the formulation of the factor of safety and up-to-date stability analyses help to unravel the issue.

Keywords: Anthropogenic loading; Coastal cliff collapse; Dynamic loading; Factor of safety; Landfill; Overloading; Pore pressure; Quick-clay landslide; Seismic loading; Stability analysis; Surcharge load; Tree load; Waste dump

Queries and Answers

Query:

Please check whether the author names and affiliations are correct.

Answer: see the correction in affiliation b

Query:

Per instruction, a Change History is mandatory for updated chapters. Please provide the name(s) of authors involved in preparing the update, and a list of the sections/figures/tables within the article that have been updated.

Answer: this is not an updated chapter but a quite next text on the same entry, written by new authors. There is thus no relation between this text and that of the first edition.

Query:

Please check if reference has to be cited in place of “and many others”.

Answer: no reference has to be provided in place of "and many others".

Query:

Per style, cross references to other articles are not allowed within the text. Hence they have been deleted.

Answer: OK

Query:

Please check if the value “2.73×10^6” has been displayed correctly.

Answer: yes, it is OK so.

Query:

Please check if the value “1.2×10^6” has been displayed correctly.

Answer: yes, it is OK so.

Query:

Please check if the value “~0.78 × 10^{6}” has been displayed correctly.

Answer: yes, it is OK so.

Query:

Please check if the value “~10.5 × 10^{3}” has been displayed correctly.

Answer: yes, it is OK so.

Query:

Please check if the value “~0.9 × 10^{6}” has been displayed correctly.

Answer: yes, it is OK so.

Query:

Please check if the value “22.5 × 10^{3}” has been displayed correctly.

Answer: yes, it is OK so.

Query:

The references ""Van den Eeckhaut et al., 2013"" occur in the reference list but not in the body of the text. Please position each reference in the text or, alternatively, delete it. Thank you.

Answer: OK. We have deleted it.